Chinese Journal of Chemical Engineering 85 (2025) 294–303

Contents lists available at ScienceDirect

Chinese Journal of Chemical Engineering

journal homepage: www.elsevier.com/locate/CJChE

Full Length Article

Preparation of magnesium phosphate cement by salt lake magnesium slag and its hydration process

Weixin Zheng [1, 2], Jinmei Dong [1, 2, *], Baolan Li [3, *], Yuanrui Li [1, 2], Qiang Wang [1, 2], Jing Wen [1, 2], Chenggong Chang [1, 2]

[1] *Key Laboratory of Comprehensive and Highly Efficient Utilization of Salt Lake Resources Qinghai Institute of Salt Lake. Chinese Academy of Sciences, Xining 810008, China*
[2] *Key Laboratory of Salt Lake Resources Chemistry of Qinghai Province, Xining 810008, China*
[3] *Qinghai Provincial Key Laboratory of Plateau Climate Change and Corresponding Ecological and Environmental Effects, Qinghai University of Science and Technology, Xining 810016, China*

ARTICLE INFO

Article history:
Received 29 December 2024
Received in revised form
10 March 2025
Accepted 6 May 2025
Available online 2 June 2025

Keywords:
Magnesium phosphate cements
Magnesium slag
Microstructure
Utilization of salt lake resources
MgO

ABSTRACT

Magnesium phosphate cements (MPC) have shown promising applications in many fields, but high raw material prices hinder their development. The production of salt lake MPC (SLMPC) from magnesium slag (MS), a byproduct of lithium extraction from salt lakes, offers significant environmental and economic advantages. In this study, a low-cost magnesia raw material was obtained through the calcination of MS, which was subsequently utilized in conjunction with KH_2PO_4 to prepare SLMPC. The changes in hydration products, microscopic morphology, solution pH value, and TG content during the SLMPC curing process, and the hydration kinetics equation and model were used to study the hydration processes of SLMPC. The results show that the outcome indicates that the SLMPC system entered the accelerated reaction stage within 6 min after mixing, where the highest heat release rate was 6.29 $J \cdot g^{-1} \cdot min^{-1}$, the maximum heat release was 205.3 $J \cdot g^{-1}$, and the main hydration product appeared at 50–60 min. The hydration behavior of SLMPC exhibits similarities to that of traditional MPC. Specifically, the acceleration phase is governed by an autocatalytic reaction, the deceleration phase is influenced by both autocatalytic reactions and diffusion processes, and the stabilization phase is predominantly controlled by diffusion mechanisms. This paper aims to establish the theoretical foundation for the industrial application of MS and the cost-effective production of MPC.

1. Introduction

Lithium is playing a critical role as an engineering material in mitigating issues that stem from the consumption of fossil fuels. For example, the application of lithium-ion batteries in an electrical vehicle and hybrid cars may minimize the potential environmental impact of pollution from conventional vehicles [1,2]. The most abundant lithium resource is continental brine, which accounts for 60% of the world's lithium reserves [3,4], and the extraction of lithium from salt lake brine is expected to become a major trend in the industry [5,6]. Lithium can be extracted from salt lake brine using several separation methodologies, such as chemical precipitation, ion exchange, liquid-liquid extraction, and membrane process [7,8]. Hydroxides and carbonates may be added to adjust the pH value of salt lake brine or precipitate Mg^{2+} during the lithium extraction process [9], and a large amount of magnesium slag (MS) will eventually be generated [10–14]. For example, 1 t of Li_2CO_3 product may be produced, producing approximately 5–7 t of MS by-product [8]. As shown in Fig. 1, the MS has a milky white block appearance.

With the gradual development of the global energy industry toward cleanliness [15], the demand for lithium resources in salt lakes has increased annually [16,17], with lithium-rich salt lakes distributed in Argentina, Chile, Bolivia, the United States, Russia, and China facing increasing environmental and resource utilization pressures [16–18]. However, public concern is growing regarding how to efficiently extract mineral elements from salt lake brine [19–22] or the environmental impact evaluation of the lithium extraction process [7,17]. However, minimal attention has been paid to the effective use of MS generated during the mineral extraction process.

* Corresponding authors.
E-mail addresses: dongda839@isl.ac.cn (J. Dong), sunnylbl@163.com (B. Li).

https://doi.org/10.1016/j.cjche.2025.05.007

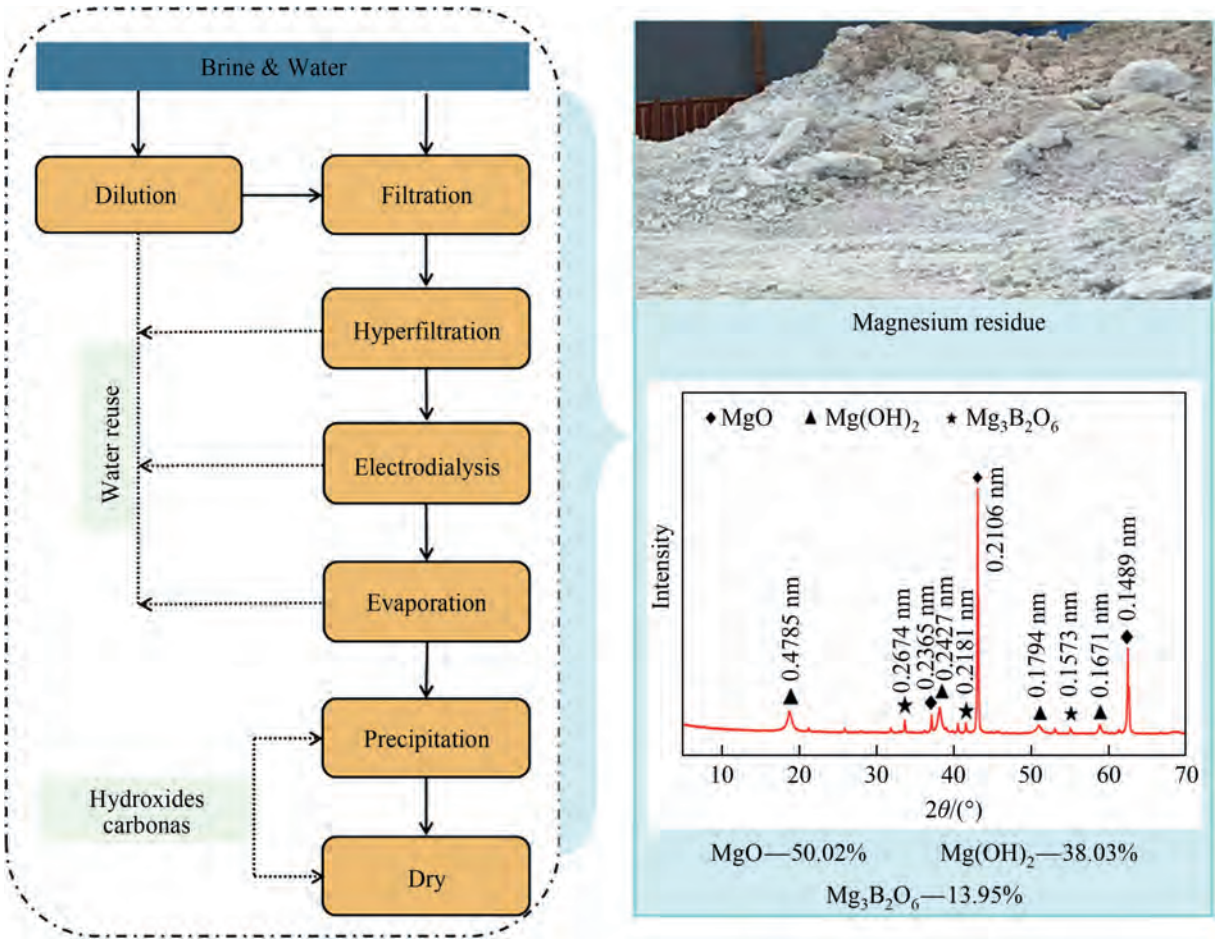

Fig. 1. System process flow of lithium extraction from salt brines.

In the use of MS as a raw material, the development of downstream products offers great significance for environment protection and the clean production and comprehensive utilization of mineral resources in Li-rich salt lake areas [16]. Therefore, it is critical to effectively use a large amount of MS without introducing other sources of pollution. MS is rich in magnesium oxide and magnesium hydroxide (exceeding 70% in total) [13,14] and may be used to prepare beneficial magnesium-based functional materials, such as magnesium hydroxide flame retardants, or high purity magnesium oxide [23,24]. However, high impurity content in MS may be a factor restricting the production of these materials with relatively high purity requirements, and an intermediate such as ammonium may be introduced or produced during the production process [25], serving as another economic and environmental challenge. The most effective strategy to use MS may involve magnesia-based cement materials [10–14]. Compared with other materials such as magnesia and magnesium hydroxide, cement materials are not highly demanding in terms of purity of raw materials and offer a high utilization rate of solid waste [26,27]. Therefore, MS, as a raw material of Mg-based cement, has high practicability and utilization value [10–14].

Magnesium phosphate cement (MPC) has the advantages of fast setting time, low shrinkage, rapid solidification, good adhesion to old concrete, small volume deformation, salt corrosion resistance, near-neutral pH, good biocompatibility, improved fixation performance, and biocompatibility with many toxic elements [28–31]. This allows MPC to be used for the rapid repair of roads, coating materials, and the curing of harmful heavy metal ions and radionuclide substances [32–34]. Using MS as a raw material to prepare environmentally friendly, inexpensive, and energy-efficient MPC materials has become significant. Tan *et al.* [12,35] and Chen *et al.* [10] discussed the feasibility of using MS as raw material for the production of magnesium phosphate cement (MKPC) with good mechanical properties and a long setting time. Dong *et al.* [36] used lithium slag to prepare MAPC mortars with better mechanical properties. MS was calcined under different conditions to obtain salt lake hard- or dead-red magnesia (SLd-MgO) in the previous work; thus, salt lake magnesium phosphate cement (SLMPC) was prepared with excellent mechanical properties and controllable setting time [11,13,14]. Notably, these studies have focused more on using magnesium slag to form suitable SLd-MgO raw materials. In addition, the involved kinetic characteristics have not been thoroughly studied, considering the hydration process of struvite ($MgKPO_4 \cdot 6H_2O$, MKP or $MgNH_4PO_4 \cdot 6H_2O$, and MAP) generated by the chemical reaction of SLd-MgO with phosphate.

Viani [37,38], Shi [39], Fan [40], Lu [41], and Mo *et al.* [42] assessed the hydration reaction processes of MPC at different hydration ages. MPC consists of an acid-base neutralization reaction between refired MgO and soluble phosphate, with the hydration reaction mechanism conforming to the through-solution mechanism [43,44]. When the mixture of MgO and soluble phosphate ($NH_4H_2PO_4$ or KH_2PO_4) makes contact with water, the soluble phosphate will first quickly dissolve to form an acidic solution. Then, the MgO particles will gradually dissociate and release Mg^{2+} in the acidic solution. This process releases a considerable amount

of heat, accompanied by autocatalysis. Finally, Mg^{2+} will react with NH_4^+/K^+ and PO_4^{3-} to form bonded crystalline phosphate hydration products, finally achieving strength [45]. The above research provides a good reference for the formation of cognitive MPC and for improving the use of MPC materials. However, these studies were based on the traditional process of d-MgO (obtained by calcination of magnesite at 1500–1700 °C [46–49]) and soluble phosphate reaction to produce MPC. Because the physical characteristics of SLd-MgO converted by MS differ from those of d-MgO, such as the specific surface area, particle size, impurity type, and content [11,13,14], it is important to determine whether the kinetic characteristics of SLd-MgO are similar to those of d-MgO in the process of forming SLMPC. Critically, the structural changes, phase changes, and thermal properties in the hydration process have not been thoroughly studied.

The hydration reaction of cement is a complex physicochemical process, and different reaction stages are controlled by different mechanisms of action. A suitable hydration reaction kinetics model can effectively explain the influence of internal and external factors on reaction rate and direction during chemical reactions, thereby revealing the macroscopic and microscopic mechanisms of chemical reactions. Therefore, in this work, X-ray diffraction (XRD), scanning electron microscopy (SEM), pH, and differential scanning calorimetry/thermogravimetric (DSC-TG) analyses were used to assess the changes in hydration products, microscopic morphology, solution pH value, and TG content during the SLMPC curing process, and the hydration kinetics equation and model were used to study the hydration processes of SLMPC. The purpose of this study was to reveal the microscopic variations and kinetic characteristics of hydration products during SLMPC curing and provide a theoretical basis for its industrial utilization.

2. Experimental

2.1. Raw materials

The MS used in this study was obtained from Qinghai Citic Guoan Group Co., Ltd (China). Chemical titration and XRD were used to analyze MS, which had main phases of MgO, $Mg(OH)_2$, and magnesium borate ($Mg_3B_2O_6$), as shown in Fig. 1. MS was calcined at 1000 °C for 3 h, then ground for 1.5 min, and passed through a 120 mesh screen to obtain the SLd-MgO raw material. The final specific surface area of SLd-MgO was 1.629 $m^2 \cdot g^{-1}$ with an average particle size of 7.13 μm. Quantitative analysis showed that the SLd-MgO, $Mg(OH)_2$, and $Mg_3B_2O_6$ contents in the SLd-MgO powder were 76.02%, 0%, and 20.44%, respectively. In addition, the content of various ions in salt lake magnesium slag before and after calcination was determined by chemical titration, as shown in Table 1. Potassium dihydrogen phosphate (KH_2PO_4; >99%) was purchased from Sinopharm Chemical Reagents Co., Ltd., dried in a drying oven at 80 °C, ground for 1–2 min, and packaged for use. Laboratory tap water was used as the curing solution.

2.2. Mix proportions and sample preparation

KH_2PO_4 was first dried for 180 min in a vacuum oven at 60 °C, then mixed with SLd-MgO, and stirred evenly. According to the design principles of the mix proportion of magnesium phosphate cement prepared from salt lake magnesium slag in existing literature, the mass ratio of SLd-MgO to KH_2PO_4 is set to 1.5:1 [50–52]. The fixed water-binder ratio was set to 0.25:1 [13,14,52]. Distilled water was added to the MKPC dry powder and quickly stirred to obtain the MKPC slurry, which was cured to different ages in an indoor environment for reserve, with a curing temperature of 20 °C ± 2 °C and humidity of 40% ± 5%.

2.3. Testing methods

2.3.1. Micro-morphology

The microstructures of the specimens were observed using an SEM (JSM-5610LV, Nippon Optical Limited, Tokyo, Japan) with a gold coating applied to the specimens, where the accelerating voltage was 20 kV, and the resolution was 3.5 nm.

2.3.2. Crystalline phase

The crushed specimens were subsequently filtered through an 80 μm sieve to prepare the powders for crystal phase analysis via powder XRD (Bruker Company, Billerica, MA, USA). The diffraction patterns were obtained using an X'Pert Pro diffractometer (PANalytical, $2\theta = 5°–70°$, Cu K_α radiation, $\lambda = 0.015406$ nm), and the Rietveld method was used to quantify the crystal phase composition by analyzing the diffraction patterns using Topas 4.2 software [53]. Furthermore, Topas 4.2 software was used to perform full spectrum fitting analysis on the existing quantitative results, and the Debye Scherrer formula was used to calculate the grain size of different substances at different reaction stages. The Debye Scherrer formula is shown in Eq. (1):

$$D = \frac{K\lambda}{B\cos\theta} \tag{1}$$

In the equation, K is the Scherrer constant. If B is the full width at half maximum of the diffraction peak, then $K = 0.89$; If B is the integral width of the diffraction peak, then $K = 1$; D is the average thickness of the grain perpendicular to the crystal plane direction (nm); B is the half width at half maximum of the diffraction peak of the measured sample; θ is the diffraction angle; λ is the wavelength of X-rays, which is 0.15406 nm.

2.3.3. pH test

The pH value of the pulp was determined using a Seven Excellence multi-parameter tester (Mettler Toledo Ltd, Switzerland), under the following test conditions. First, 20 g of MKPC powder was obtained, the slurry body-solid ratio was increased to 2:1 to produce a suspension, the temperature was controlled at 37 °C, and the slurry was stirred at a speed of 200 $r \cdot min^{-1}$ to ensure that the slurry did not precipitate. The pH value was measured at a certain set time.

2.3.4. DSC- TG test

The SDTQ600 differential scanning calorimeter (TA Instruments, USA) was used for thermal analysis of the samples. The instrument conditions were as follows: an N_2 atmosphere, a gas flow rate of 40

Table 1
Raw material analysis results of SLd-MgO (%).

	Mg^{2+}	B_2O_3	Ca^{2+}	K^+	Na^+	Cl^-	SO_4^{2-}	Li^+	Fe^{3+}	Mn^{2+}
Untreated	49.58	4.63	0.10	0.11	0.46	1.05	0.63	0.18	0.08	0.001
1000 °C, 3 h	56.35	4.10	0.14	0.11	0.28	0.21	0.67	0.12	–	–

$ml \cdot min^{-1}$, a heating rate of 10.0 °C·min^{-1}, and using Al_2O_3 as the reference material for thermal analysis.

2.3.5. Analysis of the kinetic characteristics

The hydration heat release curve of the SLMPC paste was tested using a TAM air isothermal calorimeter (TAM company, USA). The final heat release and half-life were obtained by introducing the hydration heat data into the hydration kinetics Eq. (2) proposed by Knudson [54]. The hydration time was calculated from the start of acceleration. The kinetic parameters of each stage were calculated using the kinetic Eq. (3) proposed by Kondo [55]:

$$\frac{1}{P}=\frac{1}{P_\infty}+\frac{t_{50}}{P(t-t_0)} \tag{2}$$

where P is the heat released from the acceleration period, P_∞ is the total heat released when the cement particles no longer experienced hydration, $(t-t_0)$ denotes the hydration time calculated from the start of acceleration, and t_{50} is the hydration reaction time required when the heat released from hydration reached half of the total heat (half-life):

$$\left[1-(1-a)^{1/3}\right]^N=K(t-t_0) \tag{3}$$

where a is the degree of hydration, and N is a constant related to the hydration mechanism (when $0 < N < 1$, cement hydration was controlled by the nucleation reaction; when $1 \le N < 2$, the hydration reaction was controlled by the boundary reaction; and when $N \ge 2$, the hydration reaction was controlled by the diffusion process). Additionally, K is the reaction rate constant, and $(t-t_0)$

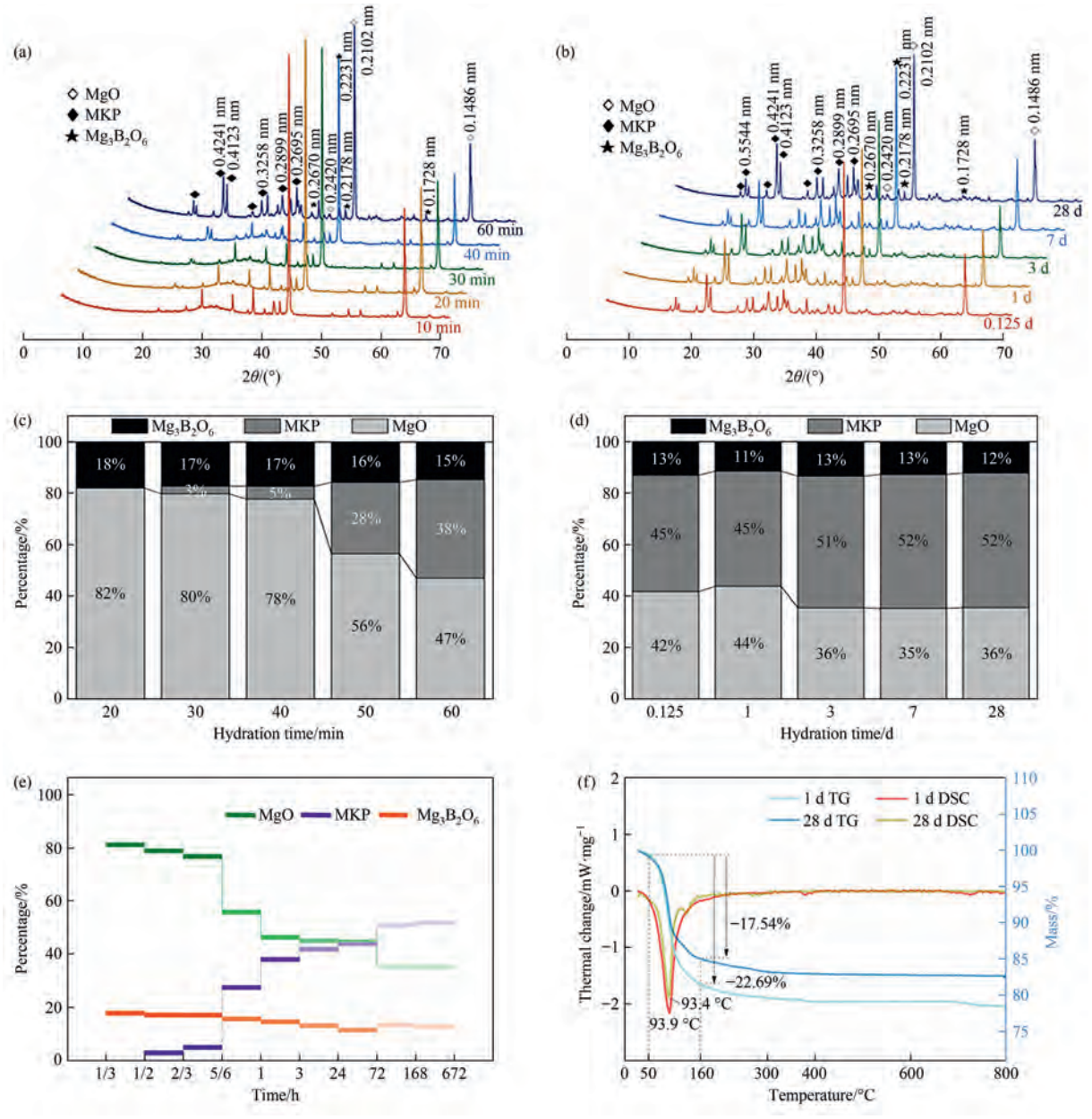

Fig. 2. Phases and their quantity in the SLMPC at various hydration times: XRD pattern (a) and quantitative analysis (c) of the SLMPC hydrated between 20 and 60 min; XRD pattern (b) and quantitative analysis (d) of SLMPC hydrated between 3 h and days; (e) change trend of the main substances in SLMPC with time; and (d) TG-DSC curves of the SLMPC sample at 1 and 28 d.

denotes the hydration time calculated from the beginning of acceleration.

3. Results and Discussion

3.1. Crystalline phase analysis and DSC-TG of SLMPC

Fig. 2(a) and (b) shows the XRD patterns of the SLMPC during short-term hydration (20–60 min) and long-term hydration (3 h to 28 d), respectively. According to Fig. 2(a), when the hydration time was less than 20 min, the main diffraction peaks in SLMPC consisted of MgO and $Mg_3B_2O_6$, and the diffraction peaks of $KMgPO_4·6H_2O$ and MKP did not appear until 30 min. The quantitative analysis of short-term hydration products using TOPAS 4.0 showed (Fig. 2(c)) that when the hydration time was less than 20 min, the main hydration products in SLMPC were MgO and $Mg_3B_2O_6$, with contents of 82% and 18%, respectively. Only at 30 min did 3% $KMgPO_4·6H_2O$ appear. As shown in Fig. 2(a), the diffraction peak of MKP did not significantly change after 40 min of hydration reaction, while a large number of MKP diffraction peaks appeared after 50 min, at which point the phase content of MKP in the system reached 28% (Fig. 2(c)). After continuous hydration to 60 min, the diffraction peak of MKP became more complete and sharp, indicating that 50–60 min was the key time point for the emergence of MKP. As hydration continued (Fig. 2(b)), the position of the MKP diffraction peak did not significantly change, and the peak strength became sharper with increasing hydration age. This indicated that the types of hydration products did not change, and the amount of hydration products constantly increased. As shown in Fig. 2(d), until 3 days (72 h) later, the MKP phase maintained a relatively stable state, and its content remained in the range of 51% ± 2%. In addition, the contents of MgO and $Mg_3B_2O_6$ in the system remained stable, maintaining a range of 12% ± 1% and 35% ± 1%, respectively.

As shown in Fig. 2(e), the growth trend of MKP phase content in the SLMPC system could be roughly divided into four steps, of which the first step was the 0–5/6 h (50 min) time range, where the MKP phase gradually formed and the corresponding MgO phase gradually decreased. The second step was in the time range of 5/6–3 h, which corresponded to the concentrated hydration reaction zone of the SLMPC system. The MKP phase content showed a trend of substantial increase, especially in the time range of 5/6–1 h, which contributed most of the increase in MKP phase content, and the corresponding MgO phase significantly decreased in this period. The third step was that in the 3–72 h time range, MKP phase growth was relatively slow, and the corresponding MgO phase decline was also relatively slow, indicating that the SLMPC system in this step interval maintained relative stability. The fourth step was the time range after 72 h, where the SLMPC system was completely cured after 72 h, obtaining a very stable phase composition.

Fig. 2(f) shows the DSC-TG curves of SLMPC hydration for 1 and 28 d. As shown in Fig. 2(f), the SLMPC at days 1 and 28 after hydration showed an obvious heat absorption peak near 93 °C, and the corresponding TG curve demonstrated obvious mass loss, which was found to be caused by the thermal dehydration of MKP, the main hydration product of SLMPC [56]. When SLMPC was hydrated for 1 day, the mass loss between 50 °C and 160 °C was 17.54% (Fig. 2(f)), while the mass loss in this interval was increased to 22.69% (Fig. 2(f)) after 28 d. The mass loss at 1 d accounted for 77.30% of the mass loss at 28 d. This is mainly because SLMPC has a very fast hydration reaction rate, which can solidify and harden within 10 min. At 1 d hydration, the solution pH stabilizes at 6.7 (Fig. 3(b)), and the hydration product MKP content accounts for 88.24% (Fig. 2(d)), indicating that the hydration reaction is basically completed at 1 d hydration and continues to hydrate in the later stage, but the hydration reaction rate significantly decreases, and hydration enters the stable period. Therefore, even if the hydration time is extended to 28 d, the quality loss of hydration products only increases by 5.15%.

3.2. Grain size variation and pH of SLMPC

The dissolution rate and pH changes of MgO in the hydration process of the SLMPC system have demonstrated a significant influence on its performance [57–59]. Fig. 3(a) shows the variation trend of MgO and MKP grain size with hydration time in SLMPC. As shown in Fig. 3(a), other than the grain size of MgO fluctuating greatly around 1 h, the remaining hydration time was stable in the range of 100–120 nm. The grain size of MKP noticeably changed with an increase in hydration time. The grain size of MKP maintained a very stable state, and its change was almost 0 before the hydration time of 2/3 h (40 min), indicating that MKP was not formed in large quantities at this time. After 2/3 h, the grain size of MKP continued to increase, reaching a maximum value at 1 h. The grain size change of MKP at 1 h was consistent with that of MgO, indicating that SLMPC system hydration was the most active during this period. After the hydration time exceeded 1 h, the grain size of MKP slightly decreased and then maintained at a relatively high level, where it essentially maintained a relatively stable state.

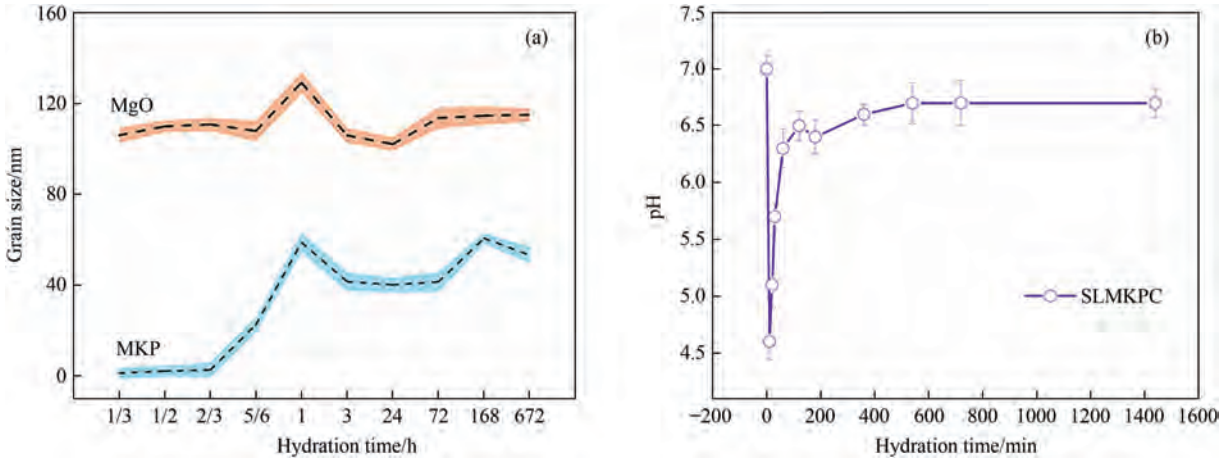

Fig. 3. Change in grain size (a) and pH (b) along with the hydration time of the SLMPC solution.

As shown in Fig. 3(b), the pH of the SLMPC solution dropped sharply in the initial stage of hydration, which appeared to be consistent with the change trend of the MPC system. MKPC essentially consisted of an acid-base neutralization reaction between refired MgO and soluble phosphate, and the hydration reaction mechanism conformed to the through-solution mechanism [57,58]. When the mixture of alkaline MgO powder particles and acidic soluble phosphate (KH_2PO_4) was in contact with water, the soluble KH_2PO_4 initially dissolved rapidly, forming an acidic solution [59], and the SLMPC system reached the lowest 4.6 after 10 min of hydration. The MgO particles gradually dissociated and released Mg^{2+} in an acidic solution [59] with extended hydration time. Therefore, the pH value of the SLMPC system rapidly increased, reaching the first peak value of 6.5 at 120 min. This process released a considerable amount of heat and was accompanied by autocatalysis. When the hydration time was greater than 120 min, the pH

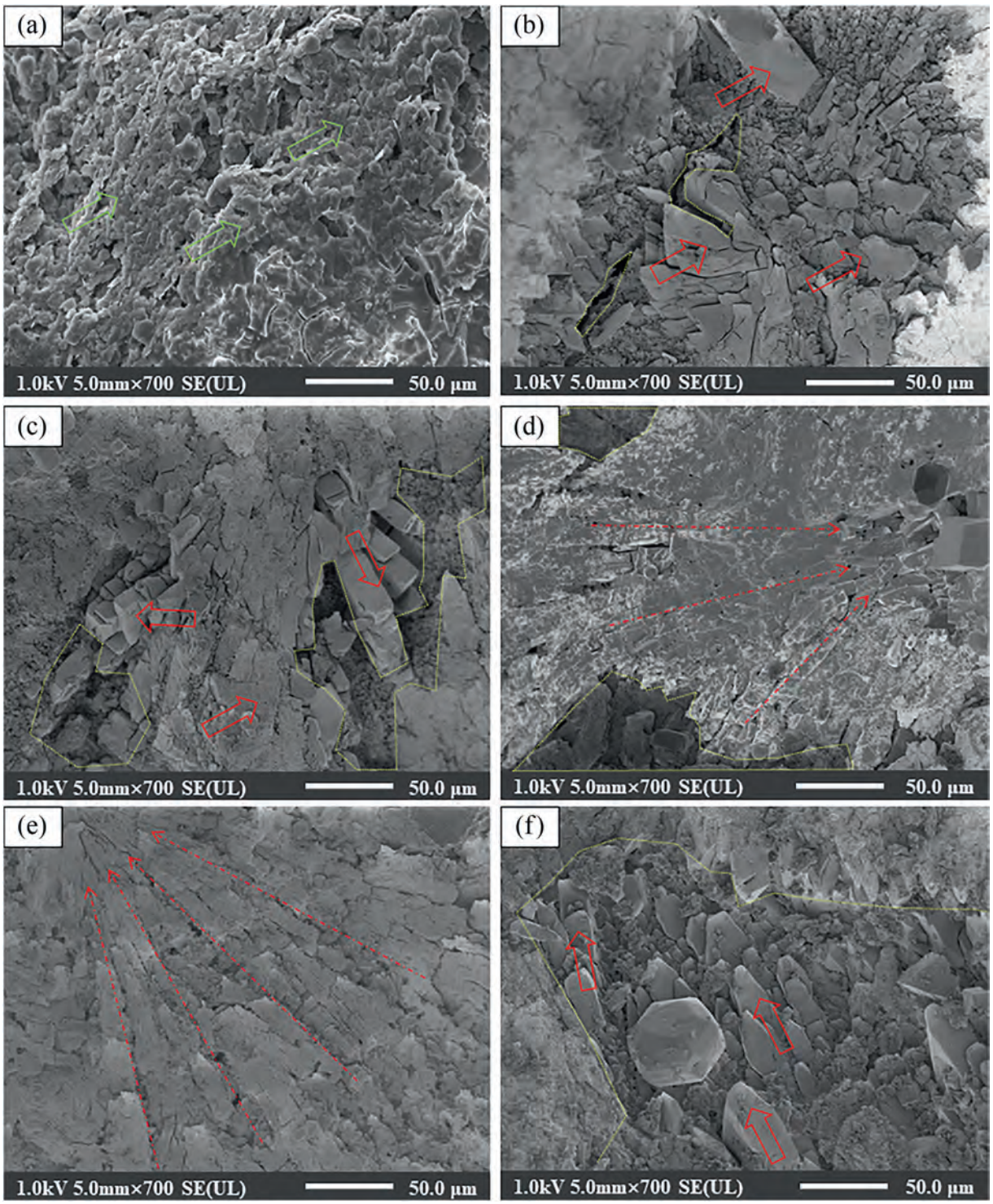

Fig. 4. SEM images of different hydration ages of the SLMPC: hydration ages of (a) 0.5 h; (b) 1 h; (c) 3 h; (d) 1 d; (e) 7 d; and (f) 28 d.

value of the system stabilized between 6 and 7 (Fig. 3(b)). The Mg^{2+}, K^+, and $PO^{3-}{}_4$ plasma reacted to form the $MgKPO_4 \cdot 6H_2O$ crystalline phosphate hydration product in this process [59].

As shown in Fig. 3(b), a violent acid-base neutralization reaction occurred inside SLMPC and the pH value reached 6.3 at 60 min in the initial stage of hydration, indicating that most of the reactions mainly occurred before 60 min. Although there was a slight fluctuation between 60 and 360 min, it still maintained a stable range (6.3 ± 0.4). After 360 min, the dissolution of MgO and the consumption of KH_2PO_4 in the SLMPC system were essentially complete or maintained a balance, and the pH value of the solution was maintained at a stable value of 6.7.

3.3. Micromorphology analysis of SLMPC

Fig. 4 shows the SEM images of the SLMPC sections at different hydration ages. When the hydration time was 0.5 h (Fig. 4(a)), the overall morphology was dominated by the gel phase, where no obvious crystal structure formed, and large pores were preserved between these gels, which provided space for later crystal development. With a hydration reaction time of 1 h, a large number of plate and prismatic crystal structures appeared in the gaps or pores of the matrix (Fig. 4(b), red arrow). Furthermore, the pore space was effectively filled during the transition from gel phase (Fig. 4(a), green arrow) to crystal phase (Fig. 4(b), red arrow), thus improving the mechanical properties of the entire matrix. However, because the development of the entire system after 1 h was incomplete, with many pores still present, this trend appeared to continue until 3 h. We observed that when the hydration age was 3 h (Fig. 4(c)), columnar crystals (red crystals) and pores (yellow regions) were found similar in shape to those after 1 h (Fig. 4(a)) of hydration in the matrix crevices or pores.

When the hydration age reached 1 day, the crystal structure in the system gradually improved, and the MKP crystals were arranged in a fan-shaped pattern (Fig. 4(d) and (e)). Although there were still some pores (yellow areas) at this time, we found that some tiny crystals were filled in the gaps. After the critical 7 d period, the microstructure of the system was similar to that observed after 1 d, with long rod-like structures and radially closely arranged crystals (Fig. 4(e)). Specifically, the microscopic morphology of the holes after the 28 d critical period was observed, and we found that the voids were filled with MKP crystals in the same orientation (Fig. 4(f)) and that the matrix structure was dense.

3.4. Kinetic characteristics analysis of SLMPC

Fig. 5 shows the hydration heat release rate and heat release curve of SLMPC at 293 K. The hydration time started when the slurry was evenly mixed and placed into the calorimeter channel, where A, B, C, and D denote the curves after each turning point. As shown in Fig. 5, the hydration heat release curve of SLMPC only contained one exothermic peak, the hydration reaction was very intense, the reaction occurred rapidly after slurry mixing, and the heat was released rapidly within a few minutes to 10 min. With the consumption of reactants and the gradual formation of products, the heat release rate decreased until the reaction was complete, and the heat release rate dropped almost to zero. The total heat release of the entire reaction process was 205.3 $J \cdot g^{-1}$. The hydration process of SLMPC could be divided into three stages, namely, I acceleration stage, II deceleration stage, and III stable stage [60,61]. Because the hydration heat release rate of SLMPC was very fast, the initial and induction periods already started and ended when the slurry was mixed in the environment. Therefore, we determined that the acceleration reaction period started before and after the slurry was placed into the calorimeter, where the acceleration period of SLMPC was 0.15–6 min, and the maximum heat release rate was 6.29 $J \cdot g^{-1} \cdot min$. The maximum heat release rate occurred for a long period of 5–13 min, where after 13.48–51.24 min, the process entered the deceleration period, the hydration heat release rate decreased, and after 95.36–456 min, the process entered the stable period.

3.5. Discussion on the characteristics of hydration kinetics of SLMPC

The M/P and pH values in the hydration process of MPC will have a great influence on the formation of its phase [60,61]. Xu *et al.* [57] studied the reaction mechanism of an MKPC system with a high magnesium-to-phosphorus ratio and found that a small amount of $Mg_2KH(PO_4)_2 \cdot 15H_2O$ was generated when the pH value of the suspension system was between 6.5 and 8.5. With an increase in pH value, it gradually transformed into MKP, and KH_2PO_4 was consumed before 30 min. Zhang *et al.* [58] determined that MKP could stably exist in solution when M/P > 0.67 and the pH value was >8.5. Rouzic *et al.* [59] studied the effect of pH on the precipitation of MKP in the suspension system of the magnesium oxide-potassium dihydrogen phosphate solution and concluded that the formation of MKP should go through three stages. Specifically, when the pH of the reaction system was <6, $MgHPO_4 \cdot 3H_2O$ first precipitated, and the slurry was in a flowing state.

When the pH of the reaction system was 6–7, $MgHPO_4 \cdot 3H_2O$ started to transform into MKP, and the slurry began to initially set. When the pH of the reaction system was greater than 7, $MgHPO_4 \cdot 3H_2O$ was completely dissolved, MKP gradually formed, and the strength of the hardened body started to develop. At least 120 min was required for KH_2PO_4 to become fully consumed for SLMPC, and when the pH value reached the first peak of 6.5, the pH value of the system stabilized between 6 and 7 (Fig. 3(b)). The reason for this difference between SLMPC and traditional MPC was directly related to the properties of the SLd-MgO raw materials (*i.e.*, the particle size (Fig. 3(a)) and the co-existence of elements such as B_2O_2, K^+, Na^+, and Cl^- (Table 1)). However, the effect of these factors on the SLMPC preparation process (compared with conventional MPC) remains unclear, especially in terms of hydration kinetics characteristics.

According to the formula of hydration kinetics (2), a fitting curve was drawn using $1/P$ and $1/(t - t_0)$, where P is the total heat release with a hydration time of $(t - t_0)$. When the straight line was extended to the vertical axis, the intercept was $1/P_\infty$, p_∞ could be obtained from the intercept, and t_{50} could be obtained from the slope of the straight line. Fig. 6 shows the $1/P - 1/(t - t_0)$ curve of

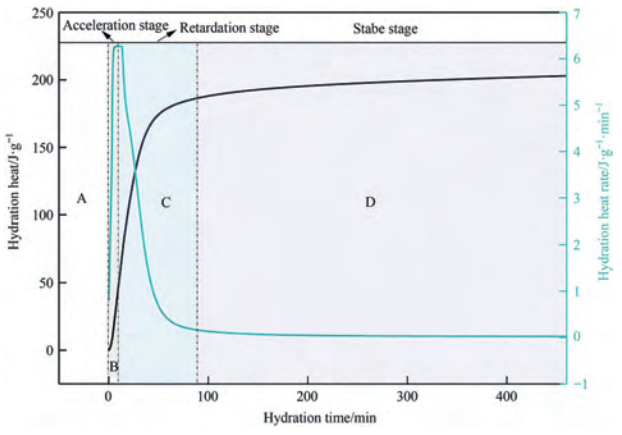

Fig. 5. Hydration heat release curve of MPC at 293 K.

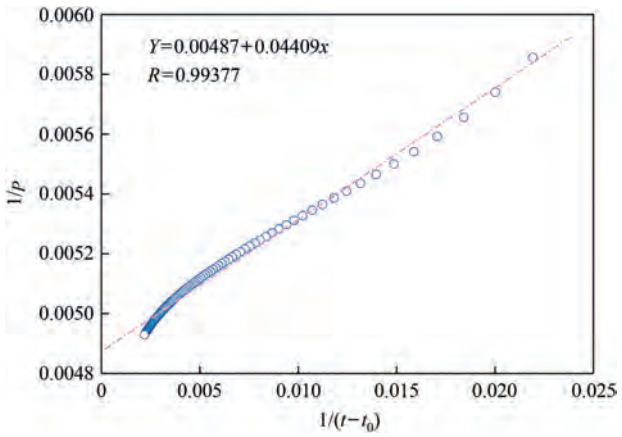

Fig. 6. Relationship between $1/P$ and $1/(t - t_0)$ of SLMPC.

the system at 293 K. Least square linear regression analysis was carried out, as shown in Fig. 6, and the hydration kinetics equation of SLMPC could be obtained by

$$\frac{1}{P} = 0.00487 + 0.04409\frac{1}{t - t_0} \tag{4}$$

The results showed that the maximum heat release P_∞ of SLMPC was 205.3 $J \cdot g^{-1}$ at 293 K, the half-life t_{50} was 9.05 min, and the correlation coefficient was $R = 0.99377$, with a good fitting effect.

To obtain the kinetic parameters of each stage of SLMPC hydration at 293 K, and to analyze the dynamic control process of each stage, the hydration kinetic model proposed by Kondo *et al.* [55] was used to fit the hydration heat release rate curve of each stage. The hydrodynamic Eq. (3) was rewritten as

$$\ln\left[1 - (1 - a)^{1/3}\right] = \frac{1}{N}\ln K + \frac{1}{N}\ln(t - t_0) \tag{5}$$

where $a = P/P_\infty$ is the degree of hydration starting from the acceleration period, and $(t - t_0)$ is the hydration time. According to Eq. (4), if $\ln[1 - (1 - a)^{1/3}]$ was used to plot $\ln(t - t_0)$, a straight line could be obtained, N could be obtained from the slope, and K could be obtained from the intercept.

Fig. 7 shows the kinetic fitting curve of SLMPC at 293 K, with Fig. 7 indicating a linear relationship between the SLMPC in the acceleration and stability periods. In the deceleration period, no linear relationship was observed between $\ln[1 - (1 - a)^{1/3}]$ and $\ln(t - t_0)$, while a linear relationship was found between $\ln[1 - (1 - a)^{1/3}]$ and $\ln(t - t_0)$. Thus, the deceleration period conformed to the formula $\ln[1 - (1 - a)^{1/3}] = K \ln t$, which was derived from Tammann's empirical formula $dx/dt = K/t$ [60,61] and was applicable to the inverse control of chemical reactions and diffusion processes. The dynamic equations of each stage are given as follows:

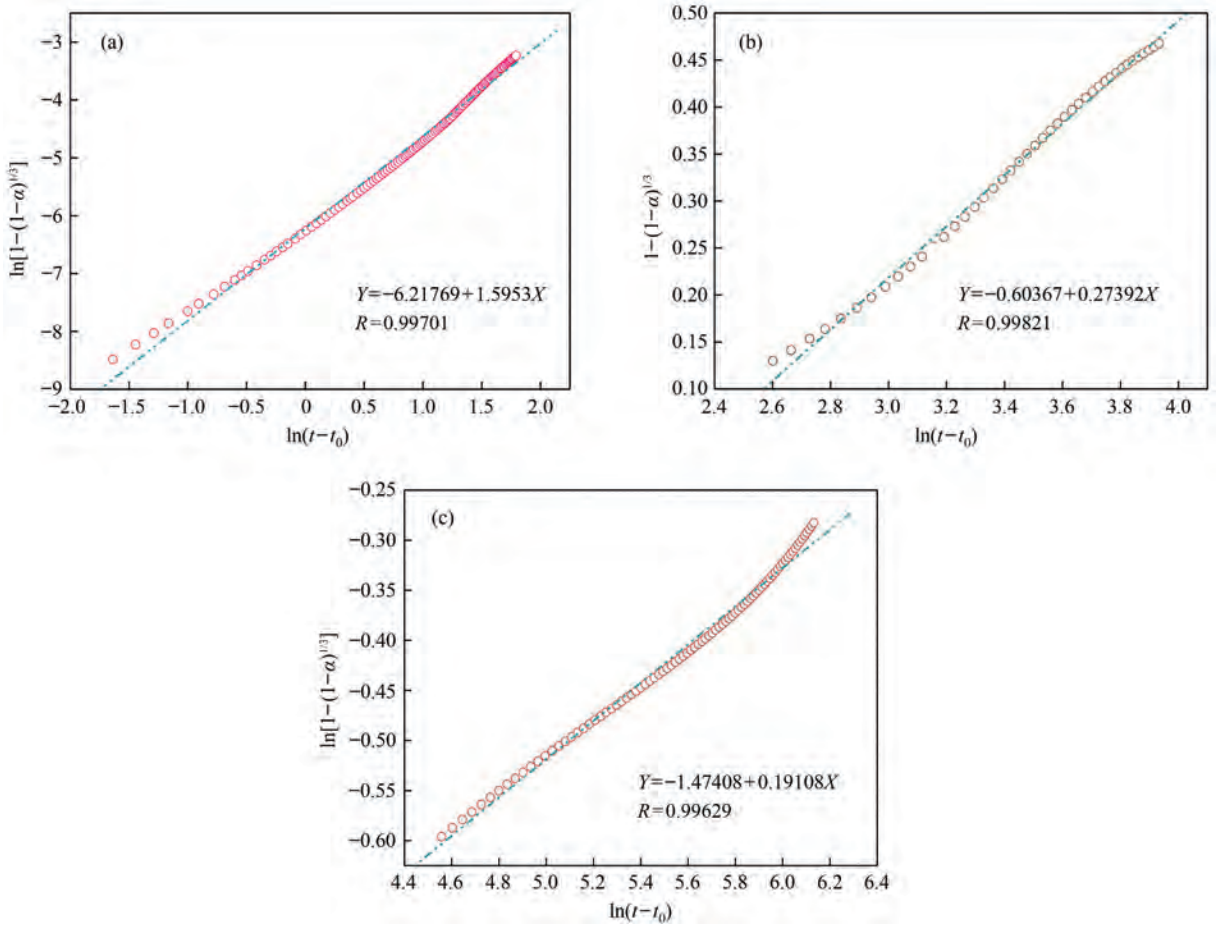

Fig. 7. Relations between $\ln[1 - (1 - a)^{1/3}]$ and $\ln(t - t_0)$ of SLMPC: (a) acceleration stage; (b) retardation stage; (c) stable stage.

Table 2
Kinetic parameters of MPC in different hydration stages.

Kinetic parameters	Acceleration stage	Retardation stage	Stable stage
Time/min	0.15–6.00	13.48–51.24	95.36–456.00
N	0.6268	–	5.2334
K	0.0203	–	0.00045

Acceleration stage (Fig. 7(a)):

$$\ln\left[1-(1-a)^{1/3}\right] = -6.21769 + 1.5953\ln(t-t_0)$$

Correlation coefficient $R = 0.99701$;
Retardation stage (Fig. 7(b)):

$$\ln\left[1-(1-a)^{1/3}\right] = -0.60367 + 0.27392\ln(t-t_0)$$

Correlation coefficient $R = 0.99821$;
Stable stage (Fig. 7(c)):

$$\ln\left[1-(1-a)^{1/3}\right] = -1.47408 + 0.19108\ln(t-t_0)$$

Correlation coefficient $R = 0.99629$.

Table 2 shows the kinetic parameters *N* and *K* of each hydration stage obtained by SLMPC at 293 K. According to the basic theory of chemical reaction kinetics [54,55], the *N* value was a constant closely related to the hydration mechanism of the cementitious system, where the larger the *N* value, the greater the resistance of the reaction and the more difficult the reaction. The reaction rate constant *K* represented the speed of reaction, where a greater reaction rate constant *K* represented an easier reaction.

By analyzing the *N* and *K* values of each stage in Table 2, and combined with the relationship between the hydration time and heat release rate in Fig. 5, the specific hydration process of SLMPC could be obtained as follows. In acceleration period B, the *n* value of MKPC was less than 1, and the reaction rate constant *k* was larger than that in the stability period, indicating that the acceleration period was controlled by the autocatalytic reaction process. In deceleration period C, the *n* value of MKP in the deceleration period was approximately equal to 1, indicating reduction. In the third stable period D, the *n* value of MKP was greater than 1, and the reaction rate constant *k* was the smallest, indicating that the stable period was mainly controlled by the diffusion process.

4. Conclusions

Lithium resources in salt lake serve as a raw material. With increasing energy demand every year, accompanied by the salt lake lithium by-product MS and other increasingly prominent solid waste problems, MS could serve as a raw material for the production of SLMPC due to its environmental and economic advantages. Therefore, in this study, we analyzed the dynamic characteristics, phase changes, and thermal properties of SLMPC during generation, and the following conclusions were obtained.

(1) The main hydration product of SLMPC was MKP, and the time point of occurrence was 50–60 min. At the beginning of precipitation, this product consisted of fine needle-like crystals. With the continued progression of the hydration reaction, the crystal structure of MKP changed from a thin rod-like, triangular-like structure to a connected compact lamellar crystal.
(2) The heat absorption peak of MKP appeared at approximately 90 °C for SLMPC, and the weight loss rate after 1 day reaches 77.3% of the 28 day mass loss rate. The hydration reaction mainly occurs in the early stage, and the reaction rate decreases in the later stage. The pH of the solution rapidly decreased and increased again at the initial stage of hydration and was stable at approximately 6.3 ± 0.4.
(3) The hydration kinetics equation of SLMPC at 293 K was $1/P = 0.00487 + 0.04409/(t-t_0)$. The mechanism of action was different in different hydration stages, with the acceleration stage controlled by autocatalytic reactions. In addition, the deceleration stage was affected by both autocatalytic reactions and diffusion, and the stability stage was controlled by diffusion.

CRediT Authorship Contribution Statement

Weixin Zheng: Writing – original draft, Resources. Jinmei Dong: Methodology, Formal analysis. Baolan Li: Writing – review & editing, Supervision. Yuanrui Li: Validation. Qiang Wang: Investigation. Jing Wen: Data curation. Chenggong Chang: Project administration.

Declaration of Competing Interest

The authors declare that they have no known competing financial interests or personal relationships that could have appeared to influence the work reported in this paper.

Acknowledgements

This work was financially supported by the Natural Science and Engineering Technology in Qinghai Province (2023), the Qinghai Province “Kunlun Talents” High end Innovation and Entrepreneurship Talent Project (2023), the Western Young Scholars Program of Chinese Academy of Sciences (2024; 2022000018), the National Natural Science Foundation of China (52404189), the Open Fund of Key Laboratory of Green and High-end Utilization of Salt Lake Resources (ISL2024-15), and, the Independent deployment project of the Qinghai Salt Lake Research Institute, CAS (E455HX3501).

References

[1] X. Hu, Z.J. Zhang, X. Zhang, Y. Wang, X. Yang, X. Wang, M. Fayena-Greenstein, H.A. Yehezkel, S. Langford, D. Zhou, B.H. Li, G.X. Wang, D. Aurbach, External-pressure–electrochemistry coupling in solid-state lithium metal batteries, *Nat. Rev. Mater.* 9 (2024) 305–320.
[2] F. Degen, M. Winter, D. Bendig, J. Tübke, Energy consumption of current and future production of lithium-ion and post lithium-ion battery cells, *Nat. Energy* 8 (2023) 1284–1295.
[3] B. Tadesse, F. Makuei, B. Albijanic, L. Dyer, The beneficiation of lithium minerals from hard rock ores: a review, *Miner. Eng.* 131 (2019) 170–184.
[4] R.M. DuChanois, A fast evaporative method for extracting lithium from brines, *Nat. Water* 1 (2023) 754–755.
[5] Y. Sun, Q. Wang, Y.H. Wang, R.P. Yun, X. Xiang, Recent advances in magnesium/lithium separation and lithium extraction technologies from salt lake brine, *Sep. Purif. Technol.* 256 (2021) 117807.
[6] X. Chen, M.Q. Yang, S.X. Zheng, F. Temprano-Coleto, Q. Dong, G.M. Cheng, N. Yao, H.A. Stone, L.B. Hu, Z.J. Ren, Spatially separated crystallization for selective lithium extraction from saline water, *Nat. Water* 1 (2023) 808–817.
[7] B.L. Li, J. Wu, J. Lu, Life cycle assessment considering water-energy nexus for lithium nanofiltration extraction technique, *J. Clean. Prod.* 261 (2020) 121152.
[8] Y.J. Zhao, X. Xiang, M. Wang, H.Y. Wang, Y. Li, J.L. Li, H.J. Yang, Preparation of LiOH through BMED process from lithium-containing solutions: effects of coexisting ions and competition between Na^+ and Li^+, *Desalination (Amst.)* 512 (2021) 115126.
[9] S.Y. Sun, L.J. Cai, X.Y. Nie, X.F. Song, J.G. Yu, Separation of magnesium and lithium from brine using a Desal nanofiltration membrane, *J. Water Process Eng.* 7 (2015) 210–217.
[10] W.H. Chen, C.Y. Wu, H.F. Yu, Y.J. Chen, S.H. Zheng, Effect of calcined MgO-rich byproduct from the extraction of Li_2CO_3 on the performance of magnesium phosphate cement, *J. Adv. Concr. Technol.* 15 (12) (2017) 749–759.

[11] W.X. Zheng, J.M. Dong, Y. Li, J. Wen, C.G. Chang, B.L. Li, Y.R. Li, Preparation technology and microstructural changes of low-activity magnesium oxide based on salt lake bischofite, *Powder Technol.* 433 (2024) 119248.

[12] Y.S. Tan, H.F. Yu, Y. Li, C.Y. Wu, J.M. Dong, J. Wen, Magnesium potassium phosphate cement prepared by the byproduct of magnesium oxide after producing Li_2CO_3 from salt lakes, *Ceram. Int.* 40 (8) (2014) 13543–13551.

[13] W.X. Zheng, J.M. Dong, J. Wen, C.G. Chang, X.Y. Xiao, Effects of water-to-cement ratios on the properties of magnesium potassium phosphate cement prepared with lithium-extracted magnesium residue, *Appl. Sci.* 11 (9) (2021) 4193.

[14] J.M. Dong, W.X. Zheng, C.G. Chang, J. Wen, X.Y. Xiao, Function and effect of borax on magnesium phosphate cement prepared by magnesium slag after salt lake lithium extraction, *Constr. Build. Mater.* 366 (2023) 130280.

[15] X. Sun, H. Hao, C. Galeazzi, T. Fishman, D.Y. Xun, M. Ericsson, G. Liu, I.L. Hsieh, Z.W. Liu, F.Q. Zhao, Reducing supply risk of critical materials for clean energy *via* foreign direct investment, *Nat. Sustain.* 7 (2024) 672–681.

[16] M.L. Vera, W.R. Torres, C.I. Galli, A. Chagnes, V. Flexer, Environmental impact of direct lithium extraction from brines, *Nat. Rev. Earth Environ.* 4 (3) (2023) 149–165.

[17] A. Alessia, B. Alessandro, V.G. Maria, V.A. Carlos, B. Francesca, Challenges for sustainable lithium supply: a critical review, *J. Clean. Prod.* 300 (2021) 126954.

[18] H.W. Li, Y. Wang, T.Y. Li, X.K. Ren, J.X. Wang, Z. Wang, S. Zhao, Nanofiltration membrane with crown ether as exclusive Li^+ transport channels achieving efficient extraction of lithium from salt lake brine, *Chem. Eng. J.* 438 (2022) 135658.

[19] X.S. Sun, X.Z. Wang, Y.L. Wan, Y.F. Guo, T.L. Deng, X.P. Yu, Synthesis of functional ionic liquids with high extraction rate and electroconductivity for lithium-magnesium separation and metallic magnesium production from salt lake brine, *Chem. Eng. J.* 452 (2023) 139610.

[20] Q.Y. Wang, M. Li, B. Zhao, B.Y. Meng, W.T. Chen, Z.K. Jiang, X. He, B. Li, X.Y. Li, L. Lin, Electricity facilitates the lithium sorption from salt-lake brine by $H_3LiTi_5O_{12}$ nanoparticles: kinetics, selectivity and mechanism, *Chem. Eng. J.* 471 (2023) 144532.

[21] S.X. Zhang, X. Wei, X. Cao, M.W. Peng, M. Wang, L. Jiang, J. Jin, Solar-driven membrane separation for direct lithium extraction from artificial salt-lake brine, *Nat. Commun.* 15 (1) (2024) 238.

[22] S.S. Xu, J.F. Song, Q.Y. Bi, Q. Chen, W.M. Zhang, Z.X. Qian, L. Zhang, S.A. Xu, N. Tang, T. He, Extraction of lithium from Chinese salt-lake brines by membranes: design and practice, *J. Membr. Sci.* 635 (2021) 119441.

[23] H.B. Dong, Z.P. Du, Y.H. Zhao, D.P. Zhou, Preparation of surface modified nano-$Mg(OH)_2$ *via* precipitation method, *Powder Technol.* 198 (3) (2010) 325–329.

[24] C. Ma, J.F. Zhang, Y.T. Liu, L.Q. Sun, Q.F. Liu, Integrated separation of precipitation and three-liquid-phase extraction for boron, lithium and magnesium from salt lake brine with high magnesium-lithium ratio, *Sep. Purif. Technol.* 347 (2024) 127541.

[25] D.X. Wang, J.Y. Zhu, R.H. Wang, Assessment of magnesium potassium phosphate cement for waste sludge solidification: macro- and micro-analysis, *J. Clean. Prod.* 294 (2021) 126365.

[26] H. Feng, L.L. Li, W.Q. Wang, Z.Q. Cheng, D.Y. Gao, Mechanical properties of high ductility hybrid fibres reinforced magnesium phosphate cement-based composites, *Compos. Struct.* 284 (2022) 115219.

[27] M. Aminul Haque, B. Chen, Y.T. Liu, S. Farasat Ali Shah, M.R. Ahmad, Improvement of physico-mechanical and microstructural properties of magnesium phosphate cement composites comprising with phosphogypsum, *J. Clean. Prod.* 261 (2020) 121268.

[28] M.A. Haque, B. Chen, Y. Maierdan, Influence of supplementary materials on the early age hydration reactions and microstructural progress of magnesium phosphate cement matrices, *J. Clean. Prod.* 333 (2022) 130086.

[29] C.Z. Li, J.C. Zhu, C.W. Yan, X.K. Meng, Experimental research on saline soil erosion resistance of magnesium phosphate cement pastes, *Constr. Build. Mater.* 341 (2022) 127752.

[30] H.L. Jiang, J.W. Zhang, T. Li, Y. Wang, Y.L. Liu, H. De Backer, Feasibility analysis of magnesium phosphate cement as a repair material for base slab of China railway track system II ballastless track, *Constr. Build. Mater.* 326 (2022) 126821.

[31] M. De Campos, C.A. Davy, N. Djelal, M. Rivenet, J. Garcia, Development of a stoichiometric magnesium potassium phosphate cement (MKPC) for the immobilization of powdered minerals, *Cem. Concr. Res.* 142 (2021) 106346.

[32] K. Gu, B. Chen, P. Yan, J.M. Wang, Recycling of phosphate tailings and acid wastewater from phosphorus chemical industrial chain to prepare a high value-added magnesium oxysulfate cement, *J. Clean. Prod.* 369 (2022) 133343.

[33] X. Cao, W.B. Wang, R. Ma, S.C. Sun, J.H. Lin, Solidification/stabilization of Pb^{2+} and Zn^{2+} in the sludge incineration residue-based magnesium potassium phosphate cement: physical and chemical mechanisms and competition between coexisting ions, *Environ. Pollut.* 253 (2019) 171–180.

[34] L.J. Gardner, C.L. Corkhill, S.A. Walling, J.E. Vigor, C.A. Murray, C.C. Tang, J.L. Provis, N.C. Hyatt, Early age hydration and application of blended magnesium potassium phosphate cements for reduced corrosion of reactive metals, *Cem. Concr. Res.* 143 (2021) 106375.

[35] Y.S. Tan, Z.B. Zhang, J. Wen, J.M. Dong, C.Y. Wu, Y. Li, D.Y. Yang, H.F. Yu, Preparation of magnesium potassium phosphate cement using by-product MgO from Qarhan Salt Lake for low-carbon and sustainable cement production, *Environ. Res.* 214 (Pt 2) (2022) 113912.

[36] P. Dong, M.R. Ahmad, B. Chen, M.J. Munir, S.M. Saleem Kazmi, Preparation and study of magnesium ammonium phosphate cement from waste lithium slag, *J. Clean. Prod.* 316 (2021) 128371.

[37] A. Viani, M. Peréz-Estébanez, S. Pollastri, A.F. Gualtieri, *In situ* synchrotron powder diffraction study of the setting reaction kinetics of magnesium-potassium phosphate cements, *Cem. Concr. Res.* 79 (2016) 344–352.

[38] A. Viani, P. Mácová, M. Peréz-Estébanez, Nucleation of amorphous precursor in magnesium phosphate cements: clues to the reaction pathway, *Mater. Lett.* 304 (2021) 130677.

[39] J. Shi, J.G. Zhao, H. Chen, P.K. Hou, S. Kawashima, J.H. Qin, X.M. Zhou, J.S. Qian, X. Cheng, Sulfuric acid-resistance performances of magnesium phosphate cements: Macro-properties, mineralogy and microstructure evolutions, *Cem. Concr. Res.* 157 (2022) 106830.

[40] S.J. Fan, B. Chen, Experimental study of phosphate salts influencing properties of magnesium phosphate cement, *Constr. Build. Mater.* 65 (2014) 480–486.

[41] Z.Y. Lu, D.S. Hou, H.Y. Ma, T.Y. Fan, Z.J. Li, Effects of graphene oxide on the properties and microstructures of the magnesium potassium phosphate cement paste, *Constr. Build. Mater.* 119 (2016) 107–112.

[42] L.W. Mo, L.M. Lv, M. Deng, J.S. Qian, Influence of fly ash and metakaolin on the microstructure and compressive strength of magnesium potassium phosphate cement paste, *Cem. Concr. Res.* 111 (2018) 116–129.

[43] N. Yang, C.J. Shi, J.M. Yang, Y. Chang, Research progresses in magnesium phosphate cement–based materials, *J. Mater. Civ. Eng.* 26 (10) (2014) 04014071.

[44] E. Soudée, J. Péra, Mechanism of setting reaction in magnesia-phosphate cements, *Cem. Concr. Res.* 30 (2) (2000) 315–321.

[45] A.J. Wang, J. Zhang, J.M. Li, A.B. Ma, L.T. Liu, Effect of liquid-to-solid ratios on the properties of magnesium phosphate chemically bonded ceramics, *Mater. Sci. Eng. C Mater. Biol. Appl.* 33 (5) (2013) 2508–2512.

[46] M.R. Ahmad, B. Chen, S. Yousefi Oderji, M. Mohsan, Development of a new bio-composite for building insulation and structural purpose using corn stalk and magnesium phosphate cement, *Energy Build.* 173 (2018) 719–733.

[47] Z. Ding, B.Q. Dong, F. Xing, N.X. Han, Z.J. Li, Cementing mechanism of potassium phosphate based magnesium phosphate cement, *Ceram. Int.* 38 (8) (2012) 6281–6288.

[48] L.M. Lv, P. Huang, L.W. Mo, M. Deng, J.S. Qian, A.G. Wang, Properties of magnesium potassium phosphate cement pastes exposed to water curing: a comparison study on the influences of fly ash and metakaolin, *Constr. Build. Mater.* 203 (2019) 589–600.

[49] X. Wang, X. Hu, J.M. Yang, L.L. Chong, C.J. Shi, Research progress on interfacial bonding between magnesium phosphate cement and steel: a review, *Constr. Build. Mater.* 342 (2022) 127925.

[50] J.H. Qin, J.S. Qian, X.B. Dai, C. You, H.Y. Ma, Z. Li, Effect of water content on microstructure and properties of magnesium potassium phosphate cement pastes with different magnesia-to-phosphate ratios, *J. Am. Ceram. Soc.* 104 (6) (2021) 2799–2819.

[51] V.M. Sglavo, F. De Genua, A. Conci, R. Ceccato, R. Cavallini, Influence of curing temperature on the evolution of magnesium oxychloride cement, *J. Mater. Sci.* 46 (20) (2011) 6726–6733.

[52] Y. LI, J.M. Dong, X.Y. Xiao, W.X. Zheng, J. Wen, C.G. Chang, Green preparation of magnesia sand and magnesium phosphate cement by utilizing common elements in salt lake as sintering aid, *Journal of Salt Lake Research* 28 (2) (2020) 15–25.

[53] J. Zhou, B.L. Li, Y.H. Lv, W.X. Zheng, Y. Shen, J.M. Dong, Y.R. Li, Q. Wang, C.G. Chang, J. Wen, Effects of Cl– and Ca2+ on the properties of magnesium oxysulfate cement, *Constr. Build. Mater* 492 (2025) 142933.

[54] T. Knudsen, On particle size distribution in cement hydration. Proceedings of 7th International Congress on the Chemistry of Cement vol. I, 1980. Paris.

[55] R. Kondo, S. Ueda, Kinetics of Hydration of Cement//5th Interna Tional Conference on the Chemistry of Cement, vols. II-4, Sess, Tokyo, 1968, pp. 203–208.

[56] S. Graeser, W. Postl, H.B. Bojar, T. Armbruster, T. Raber, K. Ettinger, F. Walter, Struvite-(K), $KMgPO46H_2O$, the potassium equivalent of struvite a new mineral, *Eur. J. Mineral* 20 (4) (2008) 629–633.

[57] B.W. Xu, F. Winnefeld, J. Kaufmann, B. Lothenbach, Influence of magnesium-to-phosphate ratio and water-to-cement ratio on hydration and properties of magnesium potassium phosphate cements, *Cem. Concr. Res.* 123 (2019) 105781.

[58] T. Zhang, H.S. Chen, X.Y. Li, Z.G. Zhu, Hydration behavior of magnesium potassium phosphate cement and stability analysis of its hydration products through thermodynamic modeling, *Cem. Concr. Res.* 98 (2017) 101–110.

[59] M. Le Rouzic, T. Chaussadent, G. Platret, L. Stefan, Mechanisms of k-struvite formation in magnesium phosphate cements, *Cem. Concr. Res.* 91 (2017) 117–122.

[60] J. Egedal, W. Fox, E. Belonohy, M. Porkolab, Kinetic simulation of the VTF magnetic reconnection experiment, *Comput. Phys. Commun.* 164 (1–3) (2004) 29–33.

[61] X.C. Fu, W.X. Shen, T.Y. Yao, Physical Chemistry, fourth ed., Higher Education Press, Peking, 2003.